

# Multi-microphone Complex Spectral Mapping for Utterance-wise and Continuous Speaker Separation

Zhong-Qiu Wang, Peidong Wang, and DeLiang Wang, *Fellow, IEEE*

**Abstract**—We propose multi-microphone complex spectral mapping, a simple way of applying deep learning for time-varying non-linear beamforming, for offline utterance-wise and block-online continuous speaker separation in reverberant conditions, aiming at both speaker separation and dereverberation. Assuming a fixed array geometry between training and testing, we train deep neural networks (DNN) to predict the real and imaginary (RI) components of target speech at a reference microphone from the RI components of multiple microphones. We then integrate multi-microphone complex spectral mapping with beamforming and post-filtering to further improve separation, and combine it with frame-level speaker counting for block-online continuous speaker separation (CSS). Although our system is trained on simulated room impulse responses (RIR) based on a fixed number of microphones arranged in a given geometry, it generalizes well to a real array with the same geometry. State-of-the-art separation performance is obtained on the simulated two-talker SMS-WSJ corpus and the real-recorded LibriCSS dataset.

**Index Terms**—Complex spectral mapping, speaker separation, microphone array processing, deep learning.

## I. INTRODUCTION

**D**RAMATIC progress has been made in talker-independent speaker separation since deep clustering [1] and permutation invariant training (PIT) [2] were proposed to address the label permutation problem. To improve separation, subsequent studies leverage spatial cues afforded by microphone arrays [3]–[7], frequency-domain phase estimation [8], time-domain optimization [9], complex ratio masking [10], and extra information such as speaker embeddings [11], [12] and visual information [13].

Our study tackles speaker separation in reverberant conditions from the angle of microphone array processing. Since target speakers are directional sources with distinct spatial origins, spatial information provides a potentially important cue for speaker separation. Conventionally, multi-microphone

beamforming followed by monaural post-filtering is the most widely adopted approach for multi-channel speech separation [14], [15]. This approach requires the accurate estimates of direction of arrival, power spectral density and spatial covariance matrix. With the recent introduction of deep learning in microphone array processing, all these estimates can now be dramatically improved. The key idea is to use DNN to identify time-frequency (T-F) units dominated by a single source and perform spatial processing based on these T-F units that contain cleaner phase. Representative work includes masking-based beamforming [16]–[18] and speaker localization [19], [20], where DNNs are trained on spectral features to estimate a T-F mask for each microphone, and the estimated masks at different microphones are then pooled to identify T-F units dominated by the same source at all the microphones for covariance matrix computation. Subsequent studies incorporate spatial features such as inter-channel phase differences (IPD) [3], [5], target direction compensated IPD [4], beamforming results [4], and stacked phases and magnitudes [21] as a way of leveraging spatial information to improve mask estimation. However, these studies aim at improving mask or magnitude estimation and do not deal with phase. In addition, they assume that these models are designed for arrays of unknown geometry. Although this generality is desirable, in real-world products such as Amazon Echo and Google Home, the number of microphones and their geometry are fixed. How to leverage fixed-array geometry is a potentially important issue for multi-channel speech processing.

Assuming fixed array geometry, we propose a multi-microphone complex spectral mapping approach for speaker separation, where the real and imaginary (RI) components of multiple microphones are input to a DNN to predict the RI components of the direct-path target speakers captured at a reference microphone. The initial separation results can be utilized to compute statistics for beamforming. The RI components of beamforming results can be combined with the RI components of multiple microphone signals for post-filtering.

Why would this approach work? We believe that, for a fixed-geometry array, the DNN could learn to enhance and separate speech arriving from a particular direction by exploiting the stable spatial information contained in multiple microphones. This approach is in a way similar to classification based sound source localization for fixed-geometry arrays [22], [23], where a DNN is trained to learn a one-to-one mapping from inter-channel phase patterns to discretized target directions. Based on deep learning, our proposed approach exploits the non-linear spatial information contained in multi-channel inputs, whereas

Manuscript received on Oct. 4, 2020. This research was supported in part by an NIDCD grant (R01 DC012048), an NSF grant (ECCS-1808932), and the Ohio Supercomputer Center.

Zhong-Qiu Wang was with the Department of Computer Science and Engineering, The Ohio State University, Columbus, OH 43210-1277 USA, while performing this work. He is now with Mitsubishi Electric Research Laboratories, Cambridge, MA 02139, USA (e-mail: [wang.zhongqiu41@gmail.com](mailto:wang.zhongqiu41@gmail.com)).

Peidong Wang is with the Department of Computer Science and Engineering, The Ohio State University, Columbus, OH 43210-1277 USA (e-mail: [wang.7642@osu.edu](mailto:wang.7642@osu.edu)).

DeLiang Wang is with the Department of Computer Science and Engineering & the Center for Cognitive and Brain Sciences, The Ohio State University, Columbus, OH 43210-1277 USA (e-mail: [dwang@cse.ohio-state.edu](mailto:dwang@cse.ohio-state.edu)).

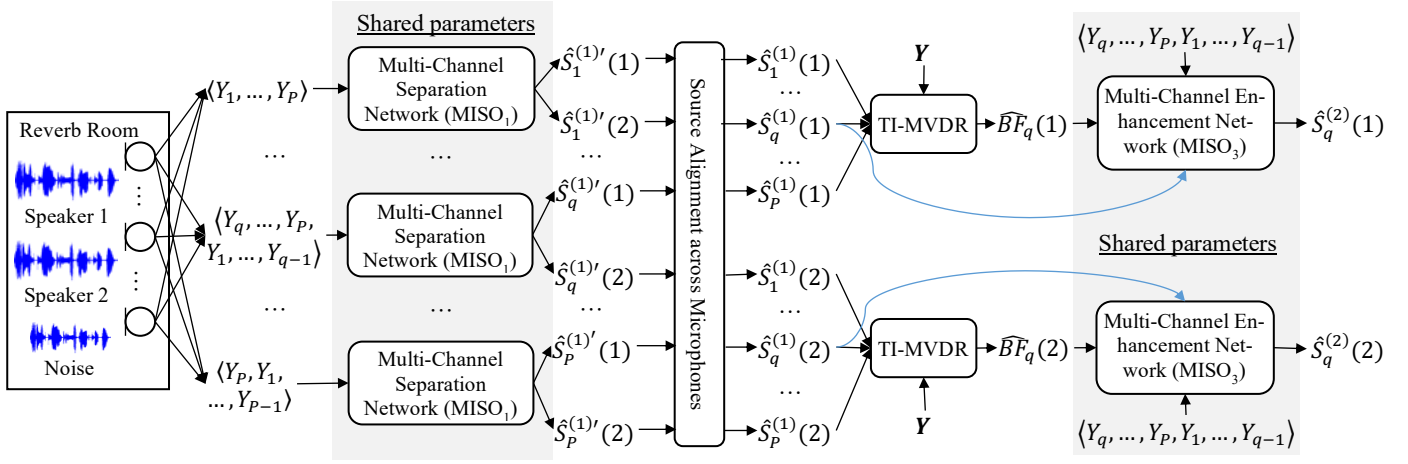


Figure 1. MISO<sub>1</sub>-BF-MISO<sub>3</sub> for two-source separation and dereverberation. The source alignment module is needed for aligning separation results across microphones, as uPIT results at different microphone may have different permutations. The prime in say  $\hat{S}_q^{(1)'}$  is used to differentiate the notation from  $\hat{S}_q^{(1)}$ , as we need to align sources across microphones before beamforming.

conventional beamforming is linear in nature and typically only utilizes second-order statistics at each frequency.

A key question is, can a DNN trained using simulated RIRs generated by an RIR simulator based on a given geometry generalize to a real array with the same geometry? An affirmative answer is far from clear, as real recordings exhibit various mismatches from training, such as channel variations and different acoustic environments. In addition, the geometry of a real array, even well calibrated, contains manufacturing imperfections, meaning that the actual geometry would be slightly different from theoretical design. Based on LibriCSS [24], a real-recorded dataset designed for continuous speaker separation, we show that our trained models generalize reasonably well to a real array, producing state-of-the-art separation on LibriCSS.

Our study makes four major contributions. First, we propose multi-microphone complex spectral mapping, a simple way of using deep learning for time-varying non-linear beamforming on fixed arrays. The proposed approach can effectively exploit spatial information contained in multiple microphones, producing clear improvement over monaural complex spectral mapping and time-invariant beamforming. Second, we integrate multi-microphone complex spectral mapping with beamforming and post-filtering for better separation. For beamforming, we design a circular shift mechanism for utilizing a single trained multi-microphone model to compute statistics for beamforming. For post-filtering, we find that enhancing target speakers one by one rather than predicting them all at once deals with reverberation better. Our experiments show that the immediate separation output from our multi-microphone models yields much better recognition results than time-invariant beamforming. Third, we demonstrate that the trained multi-microphone models generalize reasonably well to a real device. Fourth, a frame-level speaker counting module is proposed to correct erroneous separation in one-speaker segments. These contributions together lead to state-of-the-art separation performance on the public SMS-WSJ [25] and LibriCSS [24] datasets recently

constructed for utterance-wise and continuous-input speaker separation. An earlier version [26] of this study has been published in ICASSP 2020, but it only tackles speech dereverberation, not separation.

In the following sections, we present the physical model and objectives in Section II, and the proposed algorithms in Section III. Evaluation setup and results are detailed in Section IV and V. Section VI concludes this paper.

## II. PHYSICAL MODEL AND OBJECTIVES

Given a  $P$ -channel time-domain signal  $\mathbf{y}[n] \in \mathbb{R}^{P \times 1}$  recorded in a reverberant and noisy enclosure with  $C$  speakers, the physical model in the short-time Fourier transform (STFT) domain is formulated as

$$\begin{aligned} \mathbf{Y}(t, f) &= \sum_{c=1}^C \mathbf{X}(c, t, f) + \mathbf{N}(t, f) \\ &= \sum_{c=1}^C \left( \mathbf{d}_q(c, f) S_q(c, t, f) + \mathbf{H}(c, t, f) \right) + \mathbf{N}(t, f) \end{aligned} \quad (1)$$

where  $\mathbf{Y}(t, f)$ ,  $\mathbf{X}(c, t, f)$ , and  $\mathbf{N}(t, f) \in \mathbb{C}^{P \times 1}$  respectively denote the complex STFT vectors of the received mixture, reverberant image of speaker  $c$ , and reverberant noise, at time  $t$  and frequency  $f$ . Assuming that each speaker does not move within a single utterance,  $\mathbf{X}(c, t, f) = \mathbf{d}_q(c, f) S_q(c, t, f) + \mathbf{H}(c, t, f)$ , where  $S_q(c, t, f) \in \mathbb{C}$  is the complex STFT coefficient of the direct-path signal of source  $c$  captured by a reference microphone  $q$ ,  $\mathbf{d}_q(c, f)$  the time-invariant relative transfer function (RTF) of source  $c$  with respect to microphone  $q$  with the  $q^{\text{th}}$  element being one, and  $\mathbf{H}(c, t, f)$  the early reflections plus late reverberation of source  $c$ .

Our goal is to estimate  $S_q(c)$  for each source at the reference microphone based on the spectral and spatial information contained in  $\mathbf{Y}$ . We use the time-domain signals corresponding to  $S_q(c)$  for metric computation.

Our study assumes a uniform circular array geometry. This type of geometry is very common, including two-microphone linear arrays, three-microphone equilateral-triangle arrays and four-microphone square arrays. We assume the same array is used for training and testing. The first microphone on the circle is always considered as the reference microphone, i.e.  $q = 1$ .

### III. PROPOSED ALGORITHMS

Figure 1 illustrates the proposed system, i.e. MISO<sub>1</sub>-BF-MISO<sub>3</sub>, which produces the best performance in our experiments. It contains a separation network and an enhancement network. The separation network performs multi-microphone complex spectral mapping to compute initial separation results, which are then aligned across microphones and used to compute a time-invariant minimum variance distortionless response (MVDR) beamformer for each source. The beamforming results are combined with the mixture and initial separation results to train an enhancement network to enhance target speakers one by one. In the following subsections, we describe each module, alternative methods and baseline models. The last subsection presents the application of MISO<sub>1</sub>-BF-MISO<sub>3</sub> with a speaker counting module for block-online continuous speaker separation.

#### A. SISO<sub>1</sub>

We employ monaural complex spectral mapping [27] for both separation and dereverberation. We denote this method as **SISO<sub>1</sub>** (single-microphone input and single-microphone output). The key idea is to predict the RI components of direct sound from the mixture [27]. Building upon utterance-level PIT (uPIT) [2], the loss function is defined on the predicted RI components and the resulting magnitude, following [28], [29].

$$\begin{aligned} \mathcal{L}_{q,\text{uPIT}} = \min_{\psi_q \in \Psi} \sum_{c=1}^C & \left( \left\| \hat{R}_q^{(k)}(\psi_q(c)) - \text{Real}(S_q(c)) \right\|_1 \right. \\ & + \left\| \hat{I}_q^{(k)}(\psi_q(c)) - \text{Imag}(S_q(c)) \right\|_1 \\ & \left. + \left\| \sqrt{\hat{R}_q^{(k)}(\psi_q(c))^2 + \hat{I}_q^{(k)}(\psi_q(c))^2} - |S_q(c)| \right\|_1 \right) \end{aligned} \quad (2)$$

where  $\Psi$  denote the set of all the permutations of  $C$  sources,  $\psi_q$  is a permutation at microphone  $q$ ,  $\hat{R}_q$  and  $\hat{I}_q$  are the estimated RI components produced by linear activation in the output layer,  $k \in \{1, 2\}$  denotes which DNN produces the output since we will have two DNNs in our later multi-channel system,  $\text{Real}(\cdot)$  and  $\text{Imag}(\cdot)$  respectively extract the real and imaginary components,  $|\cdot|$  computes magnitude, and  $\|\cdot\|_1$  computes the  $L_1$  norm. The separation result is obtained as  $\hat{S}_q^{(k)} = \hat{R}_q^{(k)} + j\hat{I}_q^{(k)}$ . The network input is the RI components of  $Y_q$ . See Figure 4 for an illustration of network architecture.

#### B. SISO<sub>1</sub>-BF and SISO<sub>1</sub>-BF-SISO<sub>2</sub>

For multi-channel processing, we apply SISO<sub>1</sub> to each microphone and use the predicted multi-channel complex spectra to compute statistics for MVDR beamforming (denoted as

**SISO<sub>1</sub>-BF**), which will be detailed later in Section III.F. Next, the beamforming results are combined with the mixture and the SISO<sub>1</sub> separation results, all at the reference microphone, to train another SISO network to improve the separation. This second SISO network is essentially a post-filter, which performs enhancement and does not need to resolve the permutation problem. It estimates all the  $C$  speakers by using  $\langle Y_q, \hat{B}\hat{F}_q(1), \dots, \hat{B}\hat{F}_q(C), \hat{S}_q^{(1)}(1), \dots, \hat{S}_q^{(1)}(C) \rangle$  as inputs to predict  $\langle S_q(1), \dots, S_q(C) \rangle$  (denoted as **SISO<sub>1</sub>-BF-SISO<sub>2</sub>**). The loss function is defined on the predicted RI components and their resulting magnitudes, similar to Eq. (2) but without resolving permutations. Note that we use different subscripts, say SISO<sub>1</sub>-BF-SISO<sub>2</sub>, to denote different SISO models, as they take in different features and predict different targets. This convention applies to all of our models.

#### C. MISO<sub>1</sub>

In a multi-microphone setup, SISO<sub>1</sub>-BF-SISO<sub>2</sub> does not use DNNs to directly model multiple microphones. We propose **MISO<sub>1</sub>** (multi-microphone input and single-microphone output) networks for multi-channel speaker separation, where we stack the RI components of multiple microphone signals  $\langle Y_1, \dots, Y_P \rangle$  to predict the RI components of all the speakers  $\langle S_q(1), \dots, S_q(C) \rangle$  at a reference microphone  $q$  (set to the first microphone on the circle). The loss function is  $\mathcal{L}_{q,\text{uPIT}}$ .

This approach is in spirit similar to the classic multi-channel Wiener filter [14], where a linear filter is computed per T-F unit to project the mixture onto target speech. Our study trains a DNN to do this. Implicitly broadband and capable of exploiting a large context window along time and frequency by using, for example, dilated convolution, recurrence or self-attention, the DNN essentially learns to perform time-varying non-linear beamforming. Although this would be difficult to learn for unknown arrays, where test geometry differs from the trained geometry, it may work well if array geometry is the same between training and testing, as the inter-channel phase patterns do not change for signals coming from a particular direction. In such a case, the DNN would likely be able to exploit such fixed patterns for better separation than using just a single microphone. This approach is conceptually simple, computationally efficient, and can be easily modified for online real-time processing.

Different from earlier studies that explicitly encode spatial information using inter-channel phase patterns [3], [5], [7], our approach directly models the RI components of multiple microphones using a convolutional encoder-decoder neural network (see Figure 4). Note that decoupling multi-channel RI components into separate IPDs and magnitudes cannot fully leverage the power of convolutional neural networks, as decoupled features exhibit different patterns less suitable for direct convolution. As a result, typical methods [5], [7] use a fully-connected input layer (or one-dimensional convolution) to compress disparate IPDs and magnitudes into lower-dimensional fixed-length vectors, which however may lose phase information. In addition, these methods introduce many more parameters when the number of microphones increases, because of the fully-connected layer. Furthermore, they typically only consider the IPDs between a reference microphone and other microphones to reduce parameters. This may not be optimal as not all the

microphone pairs are leveraged. In contrast, our MISO networks with encoder-decoder structure perform convolution on multi-microphone RI components to exploit inter-channel phase patterns among all the microphones. The short-cut connections from the encoder to the decoder can better flow the multi-channel phase information inside the network. The increased number of parameters is negligible. For the network architecture in Figure 4, a MISO network only has  $((P - 1) \times 2) \times 16 \times 3 \times 3$  more parameters than a SISO network, where  $P$  is the number of microphones, 16 the number of feature maps in the first two-dimensional convolution,  $3 \times 3$  the kernel size, and 2 is because we stack real and imaginary components. The increased amount of computation of MISO over SISO is only from the first convolutional layer, which is negligible relative to the rest of the network.

Different from the convolutional beamformer approach [30] and approaches that use DNN to first predict beamforming filters and then perform linear filtering [31], [6], [32], our approach directly predicts target speech from multi-channel inputs in a non-linear way and is hence more parsimonious.

Although there are time-domain approaches using multi-microphone inputs and single-microphone output for speech enhancement and speaker separation [6], [33]–[36], their success in environments with significant reverberation is less impressive [37] than in anechoic conditions, and their generalization to realistic noisy-reverberant recordings is unclear. In addition, our study integrates multi-microphone complex spectral mapping with beamforming and post-filtering, which produce further improvements.

#### D. MISO<sub>1</sub>-BF

We use the initial separation results by MISO<sub>1</sub> to compute an MVDR beamformer for each source (denoted as **MISO<sub>1</sub>-BF**). Since MISO leverages multi-microphone information, it can provide better signal statistics for beamforming than SISO.

The ideal solution for time-invariant beamforming is to estimate each complex-valued source at each microphone to compute covariance matrices using Eq. (3). Since MISO<sub>1</sub> is trained on the concatenation of an ordered list of microphones  $\langle Y_1, \dots, Y_P \rangle$  to predict  $Y_1$ , at run time we cannot feed in  $\langle Y_1, \dots, Y_P \rangle$  to MISO<sub>1</sub> to estimate say  $Y_2$ . One cumbersome way would be to train another model to predict  $Y_2$ . In this way, one has to train  $P$  different models, one at each microphone. We instead circularly shift the microphones at run time for the prediction of each microphone signal, i.e. we feed  $\langle Y_p, \dots, Y_P, Y_1, \dots, Y_{p-1} \rangle$  to MISO<sub>1</sub> to predict  $S_p$  for  $p \in \{1, \dots, P\}$ . Clearly, this strategy should work if the microphones are arranged uniformly on a circle. What if microphones are not configured this way? For instance, in an Amazon Echo setup where the first  $P - 1$  microphones are on a circle and the last at the circle center. In such a case, we can circularly shift the microphones on the circle, and always put the center microphone at last in the ordered list, i.e. we use  $\langle Y_p, \dots, Y_{p-1}, Y_1, \dots, Y_{p-1}, Y_p \rangle$  to predict  $S_p$ , for  $p \in \{1, \dots, P - 1\}$ . In this case, we can only use the  $P - 1$  microphones on the circle for later beamforming, which should not be much worse than using  $P$  microphones if  $P$  is not small and the aperture sizes are the same. An alternative is to use T-F masks estimated

on the  $P - 1$  microphones to compute a pooled mask to perform mask-based beamforming on  $P$  microphones. When  $P$  is large, the quality of the pooled mask computed from  $P - 1$  masks should be very close to that computed from  $P$  masks. We leave this alternative for future investigation.

#### E. MISO<sub>1</sub>-BF-MISO<sub>2</sub> and MISO<sub>1</sub>-BF-MISO<sub>3</sub>

Similar to SISO-BF-SISO, the beamforming results  $\widehat{BF}_q$  are combined with multi-channel inputs  $\mathbf{Y}$  and initial separation results  $\hat{S}_q^{(1)}$  to train another MISO network to further predict  $S_q$  (see Figure 1). This MISO network is designed to leverage multi-microphone modeling for post-filtering. It essentially performs enhancement and does not need to resolve the permutation problem, as the problem has already been resolved by the first network. It can estimate  $C$  speakers all at once by using  $\langle Y_1, \dots, Y_P, \widehat{BF}_q(1), \dots, \widehat{BF}_q(C), \hat{S}_q^{(1)}(1), \dots, \hat{S}_q^{(1)}(C) \rangle$  as inputs to predict  $\langle S_q(1), \dots, S_q(C) \rangle$  (denoted as **MISO<sub>1</sub>-BF-MISO<sub>2</sub>**), or predict each target speaker one by one by using  $\langle Y_1, \dots, Y_P, \widehat{BF}_q(c), \hat{S}_q^{(1)}(c) \rangle$  to predict  $S_q(c)$  (denoted as **MISO<sub>1</sub>-BF-MISO<sub>3</sub>**). We find that the latter produces better separation, likely because each source has a different RIR and hence it is best to do separation separately. The downside is that the second DNN needs to be used  $C$  times at run time, once for each speaker.

#### F. MVDR Beamforming

We use estimated complex spectra to compute target and non-target covariance matrices for MVDR beamforming

$$\begin{aligned} \widehat{\Phi}(c, f) &= \frac{1}{T} \sum_t \widehat{\mathbf{S}}(c, t, f) \widehat{\mathbf{S}}(c, t, f)^H \\ \widehat{\Phi}(-c, f) &= \frac{1}{T} \sum_t \widehat{\mathbf{V}}(-c, t, f) \widehat{\mathbf{V}}(-c, t, f)^H \end{aligned} \quad (3)$$

where  $T$  is the total number of frames within a mixture or a sliding block, and  $\widehat{\mathbf{V}}(-c, t, f) = \mathbf{Y}(t, f) - \widehat{\mathbf{S}}(c, t, f)$ . It is suggested in [28], [29] that such estimated complex spectra lead to better covariance matrix estimation than real-valued masks, as long as the spectra exhibit better phase than the mixture.

As a target speaker can be viewed as a point source, we compute its steering vector  $\widehat{\mathbf{r}}(c, f)$  as follows

$$\widehat{\mathbf{r}}(c, f) = \mathcal{P}\{\widehat{\Phi}(c, f)\} \quad (4)$$

$$\widehat{\mathbf{d}}(c, f; q) = \widehat{\mathbf{r}}(c, f) / \widehat{r}_q(c, f) \quad (5)$$

where  $\mathcal{P}\{\cdot\}$  extracts the principal eigenvector. We further divide  $\widehat{\mathbf{r}}(c, f)$  by its  $q^{\text{th}}$  element to obtain an estimate of the RTF with respect to the reference microphone.

An MVDR beamformer is computed as

$$\widehat{\mathbf{w}}(c, f; q) = \frac{\widehat{\Phi}(-c, f)^{-1} \widehat{\mathbf{d}}(c, f; q)}{\widehat{\mathbf{d}}(c, f; q)^H \widehat{\Phi}(-c, f)^{-1} \widehat{\mathbf{d}}(c, f; q)} \quad (6)$$

and beamforming results are

$$\widehat{BF}_q(c, t, f) = \widehat{\mathbf{w}}(c, f; q)^H \mathbf{Y}(t, f) \quad (7)$$

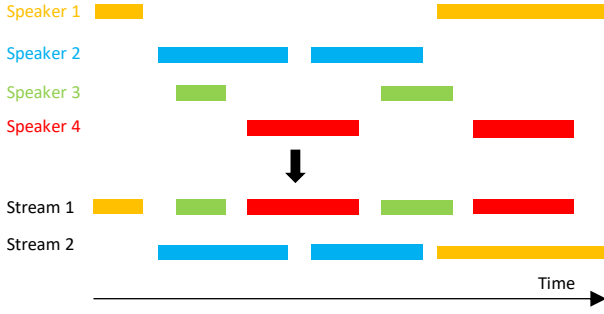


Figure 2. Task illustration of continuous speaker separation.

We consider time-invariant beamforming, as recent studies [29], [38] show that time-varying beamforming does not lead to clear improvement for post-filtering when sources do not move.

### G. Block-online MISO<sub>1</sub>-BF-MISO<sub>3</sub> for CSS

Continuous-input speaker separation [24] deals with the scenario where signals from an unknown number of speakers, possibly degraded by reverberation, noise and various degrees of speaker overlap, come as a continuous stream. Following [24], we focus on separating the input stream into two streams, each being enhanced and free of concurrent speech, as illustrated in Figure 2. This processing can be useful for streaming for example conversational speech recognition systems.

We follow the overlap-block idea proposed in [24], [39] for block-online continuous speaker separation. Figure 3 illustrates this idea. The MISO-BF-MISO model is applied to each block independently, i.e. considering each block as a separate mixture and not using any information from future frames, to get separation results. Speaker tracking or block stitching is performed based on the separation results of the overlapped frames between consecutive blocks. The inevitable delay is the block shift size if a non-causal model is applied in each block. Following [24], we assume that each short block (in our study 2.424 s) contains at most two speakers. This is a reasonable assumption in meeting scenarios as long as turn taking does not happen frequently.

We empirically observed that when a model trained on two-speaker mixtures is applied to process one-speaker utterances, it sometimes splits the single speaker to two streams, possibly because the model is trained to always produce two outputs. To deal with this issue, we introduce a frame-level speaker counting module to (1) count the number of speakers at each frame of the current block; (2) find segments of frames containing only one speaker based on the frame-level counting results; (3) merge the stream with weaker energy to the other stream for each detected segment of frames within the block; and (4) suppress the weaker-stream segment by multiplying it with a small constant. We perform three-class classification (i.e. zero, one or two speakers). The speaker counting branch is a Softmax layer on top of the TCN module (see Figure 4). It is trained using cross-entropy together with MISO in multi-task learning. In our simulated reverberant two-speaker validation set for LibriCSS, the accuracy of frame-level speaker counting produced by seven-channel MISO is around 97%, which is quite accurate.

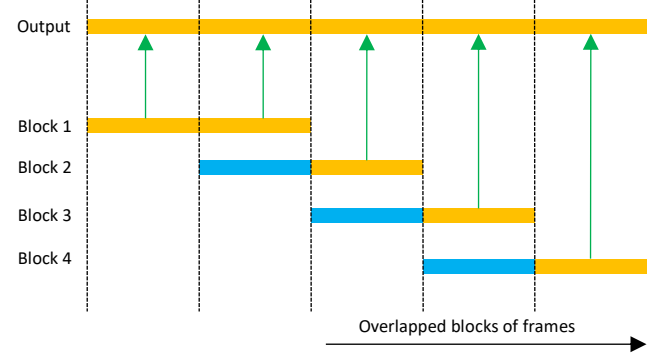


Figure 3. Illustration of block-online continuous speaker separation. Blocks in blue are used for block stitching.

Many complex-domain studies for speech enhancement only use RI components as network inputs [27], [40], [41], [28], [29], [42], because magnitude information could be learned automatically inside the model. Our study finds that incorporating mixture magnitudes for model training produces more robust separation for real-recorded mixtures in LibriCSS, possibly because the pattern of magnitudes is stabler than RI components (or waveforms) [8]. In addition, magnitude features are found to produce much more robust speaker counting in real-recorded data, as phase would not be as discriminative for speaker counting as magnitude. We only consider the magnitude at the reference microphone, as in far-field conditions, inter-channel level differences are negligibly small for compact arrays. More specifically, for example for MISO<sub>1</sub>, we use  $\langle Y_1, \dots, Y_p, |Y_q| \rangle$  to predict  $\langle S_q(1), \dots, S_q(C) \rangle$ . Adding this feature only introduces  $1 \times 16 \times 3 \times 3$  more parameters to our network (see Figure 4).

## IV. EXPERIMENTAL SETUP

Our algorithms are evaluated on two datasets, SMS-WSJ [25] and LibriCSS [24]. The first one is for two-talker separation in simulated and matched reverberant conditions, and the second for continuous speaker separation in real-recorded and unmatched reverberant conditions, both containing weak environmental noise.

SMS-WSJ [25] contains two-speaker mixtures in reverberant conditions. The sampling rate is 8 kHz. The clean sources are drawn from the WSJ0 and WSJ1 datasets. The database contains 33,561, 982, and 1,332 two-speaker mixtures for training, validation, and testing, respectively. The array is circular with six microphones uniformly spaced on a circle with 10 cm radius. The speaker-to-array distance is sampled from the range [1.0, 2.0] m, and the reverberation time (T60) is drawn from the range [0.2, 0.5] s. A weak white noise is added to simulate sensor noises. For ASR, we use the default backend acoustic model, which is trained by using single-speaker reverberant-noisy speech as inputs, and the clean alignments of its corresponding direct sound as labels. A default task-standard trigram language model is used for decoding. For separation, we consider direct sound as the training target and perform both dereverberation and separation. This is different from the official SMS-WSJ setup, which considers direct sound plus early reflections as the target for metric computation. We think that this modification



is reasonable for ASR tasks, as early reflections smear spectral patterns, although not as severely as late reverberation. It also aligns with beamforming, as beamforming methods are designed for extracting point sources.

LibriCSS [24] contains ten hours of conversational speech data recorded by playing LibriSpeech signals through loud speakers in reverberant rooms. The sampling rate is 16 kHz. The task is to perform conversational speech recognition with room reverberation and a wide range of speaker overlaps. There are ten one-hour sessions, each consisting of six ten-minute mini-sessions with different speaker overlap ratios ranging from 0% to 40%, including 0S (no overlap with short inter-utterance silence between 0.1 and 0.5 seconds), 0L (no overlap with long inter-utterance silence between 2.9 and 3.0 seconds), and 10%, 20%, 30% and 40% overlaps. The recording device has seven microphones, with six of them uniformed arranged on a circle with a 4.25 cm radius, and one at the circle center. The distance between loud speakers to the array ranges from 33 cm to 409 cm. This dataset contains two kinds of ASR evaluations, utterance-wise evaluation and continuous-input evaluation, both expecting frontend processing to produce two streams. The former assumes that each utterance has been accurately segmented and the goal is to recognize the segmented utterance. The ASR backend scores both streams and the one with lower WER is considered the final WER. The latter segments each mini-session to 60- to 120-second long segments, each with 8 to 10 utterances from at most eight speakers. The goal is to recognize all the utterances in each segment. The ASR backend scores both streams, but combines the two decoding results to compute the final WER. This is different from the utterance-wise setup, where the lower WER is picked. As a result, in one-speaker segments the continuous setup requires one stream to contain the speaker and the other to be completely silent.

Since LibriCSS only contains testing data, we need to simulate training and validation data for separation by ourselves. Our training data includes 76,750 (~129 hours) seven-channel two-speaker mixtures with moderate room reverberation and weak air conditioning noise. Among all the frames, 12% contain no speaker, 55% one speaker and 33% two speakers. We sample clean source signals from the *train-clean*-{100,360} set of LibriSpeech. Assuming the array geometry of the LibriCSS recording device, we use an RIR generator<sup>1</sup>, which is based on the image method, to simulate seven-microphone RIRs. T60 is sampled from the range [0.2,0.6] s. The average distance between speaker and array center is sampled from [0.75,2.5] m. The two speakers are ensured to be at least 10° apart and their energy level relative to each other is sampled from the range [-5,5] dB. We sample an air conditioning noise from the REVERB corpus for each reverberant two-talker mixture. The SNR between the anechoic two-source mixture and the noise is drawn from the range [5,25] dB.

The labels used for training the speaker counting branch are obtained by first applying a pre-trained DNN based voice activity detector<sup>2</sup> to the spatialized anechoic signal of each one of the two speakers at the reference microphone, and then combining the two VAD results to get the number of speakers at each frame.

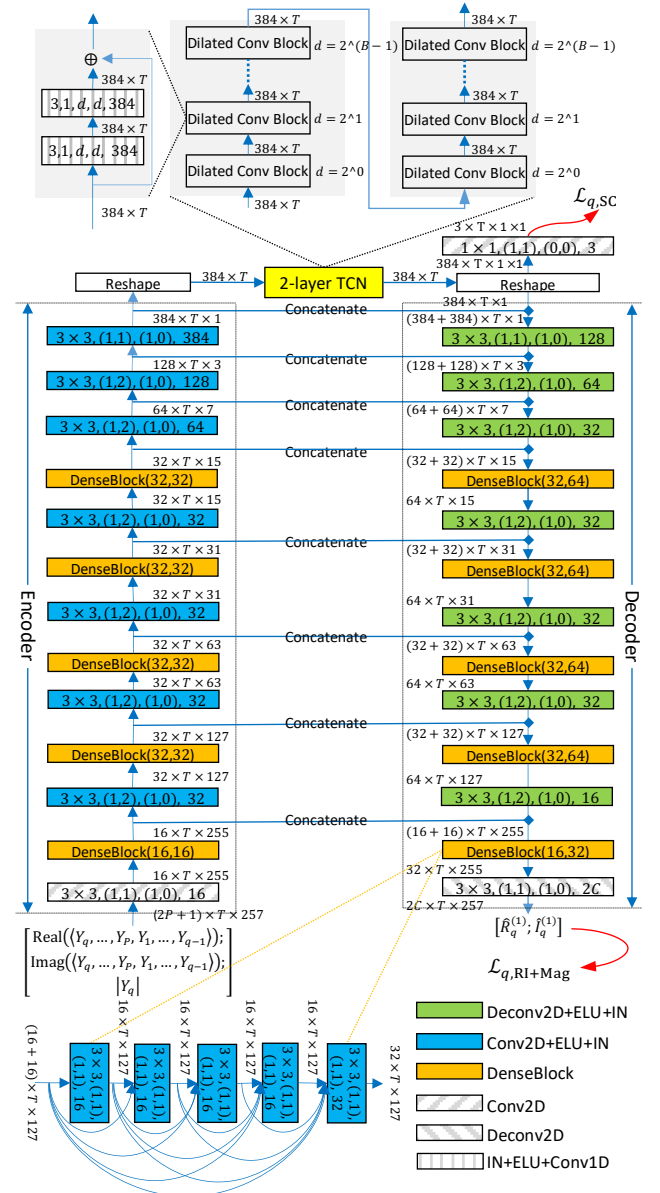


Figure 4. Network architecture of MISO<sub>1</sub> for speaker counting and predicting RI components of  $S_q$  from multi-channel inputs and  $|Y_q|$ . The tensor shape after each encoder-decoder block is in the format: *featureMaps*×*timeSteps*×*frequencyChannels*. Each one of Conv2D, Deconv2D, Conv2D+ELU+IN and Deconv2D+ELU+IN blocks is specified in the format: *kernelSizeTime*×*kernelSizeFreq*, (*stridesTime*, *stridesFreq*), (*paddingsTime*, *paddingsFreq*), *featureMaps*. Each DenseBlock( $g_1, g_2$ ) contains five Conv2D+ELU+IN blocks with growth rate  $g_1$  for the first four layers and  $g_2$  for the last layer. The tensor shape after each TCN block is in the format: *featureMaps*×*timeSteps*. Each IN+ELU+Conv1D block is specified in the format: *kernelSizeTime*, *stridesTime*, *paddingsTime*, *dilationTime*, *featureMaps*.

Following [24], [43], we set the run-time block size to 2.424 seconds for the continuous-input evaluation. It corresponds to 300 frames as our STFT window size is 32 ms and window shift is 8 ms. The block shift is set to 1.2 seconds. This means that

<sup>1</sup>[Online]. Available at: <https://github.com/ehabets/RIR-Generator>.

<sup>2</sup>[Online]. Available at: <https://kaldi-asr.org/models/m4>.

TABLE I  
SI-SDR, PESQ, eSTOI AND WER ON SMS-WSJ TEST SET.

Approaches	Use $ Y_q $ ?	SI-SDR (dB)		PESQ		eSTOI (%)		WER (%)	
#mics	-	1	6	1	6	1	6	1	6
Unprocessed	-	-5.5	-	1.78	-	44.1	-	78.42	-
SISO <sub>1</sub>	No	5.1	-	2.71	-	74.6	-	28.28	-
SISO <sub>1</sub> -BF		-	4.5	-	2.33	-	69.7	-	31.36
SISO <sub>1</sub> -BF-SISO <sub>2</sub>		-	11.2	-	3.36	-	89.5	-	10.99
MISO <sub>1</sub>		-	9.7	-	3.18	-	86.6	-	12.95
MISO <sub>1</sub> -BF		-	5.8	-	2.37	-	71.8	-	28.71
MISO <sub>1</sub> -BF-MISO <sub>2</sub>		-	13.5	-	3.48	-	91.8	-	9.45
MISO <sub>1</sub> -BF-MISO <sub>3</sub>		-	<b>15.4</b>	-	<b>3.66</b>	-	<b>94.1</b>	-	<b>8.52</b>
1ch DP-RNN [45]	-	6.5	-	2.59	-	73.4	-	38.12	-
6ch FaSNet + TAC + joint + 4ms [6]	-	-	8.8	-	2.67	-	77.5	-	27.56
6ch spatial clustering (cACGMM) [25]	-	-	-	-	-	-	-	-	39.00
6ch spatial clustering (cACGMM) + MVDR [25]		-	-	-	-	-	-	-	18.70
Oracle direct sound + early reflections	-	-	-	-	-	-	-	7.04	-
Oracle monaural SMM ( $ S_q / Y_q $ )		1.8	-	3.37	-	90.4	-	6.74	-
Oracle monaural PSM ( $ S_q \cos(\angle S_q - \angle Y_q)/ Y_q $ )		6.0	-	3.58	-	90.2	-	6.51	-
Oracle direct sound		-	-	-	-	-	-	6.40	-

our block-online system has a 1.2-second inherent delay, as in [24], [43]. For the utterance-wise evaluation, at run time we use this overlapped-block idea for the first network, as the speaker in a segmented utterance could overlap with the preceding and the succeeding speakers, while we use full-utterance information for beamforming and post-filtering.

For offline processing, we normalize the sample variance of each multi-channel signal to one before any processing. This can deal with random gains in mixtures, and would be important for mapping based methods [28], [29]. For block-online processing, we compute sample variance online, i.e. using all the samples up to the current block to normalize the current block. After obtaining the separation results at the current block, we reverse the normalization to recover the original levels before stitching. We normalize input features globally to zero mean and unit variance. When performing global normalization on RI components, the mean is simply set to zero due to the randomness of phase, and the statistics for standard deviation is collected from both the real and imaginary components within each frequency so that the phase remains the same after scaling RI components. Note that scaling RI components using different factors modifies the underlying phase.

For STFT, the window size is 32 ms, the shift is 8 ms, and the analysis window is the square root of Hann window. We use 512-point discrete Fourier transform (DFT) to extract 257-dimensional complex spectra for 16 kHz sampling rate, and 256-point DFT to extract 129-dimensional complex spectra for 8 kHz sampling rate.

Figure 4 shows the network architecture, which is a temporal convolutional network (TCN) clamped by a U-Net and includes an encoder for down-sampling and a decoder for up-sampling along frequency. We add DenseNet blocks at multiple frequency scales in the encoder and decoder. The motivation of this network design is that U-Net can maintain local fine-grained structure via its skip connections and model contextual information along frequency through down- and up-sampling. TCN can leverage long-range information by using dilated

convolutions along time, and DenseNet blocks encourage feature re-use and improve discriminability. We stack RI components as features maps in the network input and output. Similar network architectures have shown strong performance in a number of tasks including speaker separation [10], speech dereverberation [28], [26] and speech enhancement [29]. Each SISO or MISO network contains around 6.9 million parameters. We note that reducing model size is not a focus of this study.

As our study focuses on separation, we mainly use the default ASR backend in LibriCSS for recognition to facilitate comparisons with or by other studies. We also employ a more powerful end-to-end ASR backend to improve recognition on the utterance-wise task. We feed resynthesized signals to backends for recognition.

For evaluation metrics, we use scale-invariant signal-to-distortion (SI-SDR), perceptual evaluation of speech quality (PESQ), extended short-time objective intelligibility (eSTOI) and word error rates (WER) for SMS-WSJ, and report WER for LibriCSS.

## V. EVALUATION RESULTS

TABLE I reports the performance of single- and multi-channel separation and dereverberation on SMS-WSJ, along with oracle results such as direct sound, direct sound plus early reflections, spectral magnitude mask (SMM) and phase-sensitive mask (PSM). We observe clear improvement using MISO<sub>1</sub> over SISO<sub>1</sub> (9.7 vs. 5.1 dB SI-SDR), suggesting that MISO is capable of exploiting spatial information on fix-geometry arrays. Comparing MISO<sub>1</sub>-BF and SISO<sub>1</sub>-BF (5.8 vs. 4.5 dB SI-SDR), we find that MISO<sub>1</sub> produces better statistics for beamforming over SISO<sub>1</sub>. By using MISO for post-filtering, MISO<sub>1</sub>-BF-MISO<sub>2</sub> produces much better performance over MISO<sub>1</sub> and MISO<sub>1</sub>-BF (13.5 vs. 9.7 and 5.8 dB SI-SDR), and is 2.3 dB better than SISO<sub>1</sub>-BF-SISO<sub>2</sub> (13.5 vs. 11.2 dB), indicating the benefit of replacing the two single-microphone networks in SISO-BF-SISO with MISO. By predicting target speakers one by one,

TABLE II  
WER (%) ON LIBRICSS (UTTERANCE-WISE EVALUATION, 7CH).

Approaches	Use $ Y_q $ ?	ASR Backend	Overlap Ratio (%)					
			0S	0L	10	20	30	40
Unprocessed	-	Default	11.8	11.7	18.8	27.2	35.6	43.3
MISO <sub>1</sub>	No		9.0	9.1	9.6	10.7	12.0	13.4
MISO <sub>1</sub>	Yes		6.8	7.1	7.9	10.2	11.6	13.8
MISO <sub>1</sub> -BF-MISO <sub>3</sub>	Yes		5.5	5.9	5.9	6.7	7.7	8.6
MISO <sub>1</sub> -BF-MISO <sub>3</sub>	Yes	Our E2E	<b>3.0</b>	<b>3.4</b>	<b>3.2</b>	<b>4.0</b>	<b>4.8</b>	<b>4.6</b>
Chen <i>et al.</i> [24]	-	Default	8.3	8.4	11.6	16.0	18.4	21.6
Chen <i>et al.</i> [24]	-	Our E2E	3.5	3.8	4.4	6.2	8.3	9.9
Chen <i>et al.</i> [43]	-	Default	7.2	7.5	9.6	11.3	13.7	15.1
Chen <i>et al.</i> [43]	-	E2E [49]	3.1	<b>3.3</b>	3.7	4.8	5.6	6.2
Oracle anechoic speech	-	Default	4.9	5.1	-	-	-	-

TABLE III  
WER (%) ON LIBRICSS (UTTERANCE-WISE EVALUATION, 1CH).

Approaches	Use $ Y_q $ ?	ASR Backend	Overlap Ratio (%)					
			0S	0L	10	20	30	40
Unprocessed	-	Default	11.8	11.7	18.8	27.2	35.6	43.3
SISO <sub>1</sub>	No		15.5	16.3	17.3	20.8	25.4	29.4
SISO <sub>1</sub>	Yes		9.5	8.9	11.9	15.9	20.6	23.9
SISO <sub>1</sub> -SISO <sub>3</sub>	Yes		9.5	9.0	11.6	14.9	19.2	22.7
SISO <sub>1</sub> -SISO <sub>3</sub>	Yes	Our E2E	<b>4.9</b>	<b>5.1</b>	<b>6.7</b>	<b>9.4</b>	<b>12.7</b>	<b>15.5</b>
Chen <i>et al.</i> , [24]	-	Default	12.7	12.1	17.6	23.2	30.5	35.6
Chen <i>et al.</i> , [43]	-		12.9	12.2	15.1	20.1	24.3	27.6
Chen <i>et al.</i> , [43]	-	E2E [49]	5.4	<b>5.0</b>	7.5	10.7	13.8	17.1

MISO<sub>1</sub>-BF-MISO<sub>3</sub> further improves SI-SDR to 15.4 dB, amounting to 1.9 dB improvement over MISO<sub>1</sub>-BF-MISO<sub>2</sub> (15.4 vs. 13.5 dB), 10.3 dB improvement over single-channel processing (15.4 vs. 5.1 dB), and 20.9 dB improvement over no processing (15.4 vs. -5.5 dB). Similar trends are observed from PESQ, eSTOI and WER results. MISO<sub>1</sub>-BF-MISO<sub>3</sub> yields 8.52% WER, which is very close to the 6.4% WER obtained by using the oracle direct sound of each source for decoding. Our algorithm shows much better WER over conventional spatial clustering based on complex angular central GMM (cACGMM) with or without further MVDR beamforming (8.52% vs. 18.7% and 39.0% WER). These results demonstrate the outstanding effectiveness of our proposed algorithms on fixed-geometry arrays. We also provide results of representative single- and multi-channel time-domain approaches, which are popular in speaker separation. They are implemented using the recent Asteroid toolkit [44]. Compared with monaural DP-RNN [45], an improved version of Conv-TasNet [9], our SISO<sub>1</sub> model shows clearly better PESQ and WER (2.71 vs. 2.59 and 28.28% vs. 38.12%) and slightly better eSTOI (74.6% vs. 73.4%), and worse SI-SDR (5.1 vs. 6.5 dB) which is a time-domain metric. Our multi-channel models such as MISO<sub>1</sub> and MISO<sub>1</sub>-BF-MISO<sub>3</sub> produce much better performance on all the four metrics over FaSNet with TAC modules [6] (9.7 and 15.4 vs. 8.8 dB in SI-SDR, 3.18 and 3.66 vs. 2.67 in PESQ, 86.6% and 94.1% vs. 77.5% in eSTOI, and 12.95% and 8.52% vs. 27.56% in WER), a representative time-domain beamforming technique extending DP-RNN based TasNet for multi-channel separation.

TABLE II presents utterance-wise evaluation results on the seven-microphone task of LibriCSS. We observe that using

TABLE IV  
WER (%) ON LIBRICSS (CONTINUOUS-INPUT EVALUATION, 7CH).

Approaches	Use $ Y_q $ ?	ASR Backend	Overlap Ratio (%)					
			0S	0L	10	20	30	40
Unprocessed	-	Default	15.4	11.5	21.7	27.0	34.3	40.5
MISO <sub>1</sub>	No		14.4	17.4	13.7	14.7	15.7	16.9
MISO <sub>1</sub> +SC	No		9.4	10.7	10.5	11.8	14.3	16.4
MISO <sub>1</sub>	Yes		10.0	12.1	10.1	11.9	14.0	15.6
MISO <sub>1</sub> +SC	Yes		7.9	8.8	9.0	10.6	13.0	15.3
MISO <sub>1</sub> +SC-BF-MISO <sub>3</sub>	Yes		<b>6.9</b>	<b>7.2</b>	<b>7.2</b>	<b>7.9</b>	<b>9.0</b>	<b>10.4</b>
Chen <i>et al.</i> [24]	-	Default	11.9	9.7	13.4	15.1	19.7	22.0
Chen <i>et al.</i> [43]	-		11.0	8.7	12.6	13.5	17.6	19.6

TABLE V  
WER (%) ON LIBRICSS (CONTINUOUS-INPUT EVALUATION, 1CH).

Approaches	Use $ Y_q $ ?	ASR Backend	Overlap Ratio (%)					
			0S	0L	10	20	30	40
Unprocessed	-	Default	15.4	11.5	21.7	27.0	34.3	40.5
SISO <sub>1</sub>	No		15.7	17.0	17.1	20.2	24.6	27.4
SISO <sub>1</sub> +SC	No		10.5	11.5	13.5	17.3	22.0	25.8
SISO <sub>1</sub>	Yes		12.5	17.4	13.4	16.4	20.8	23.7
SISO <sub>1</sub> +SC	Yes		<b>9.8</b>	9.5	<b>11.9</b>	16.0	20.5	23.6
SISO <sub>1</sub> +SC-SISO <sub>3</sub>	Yes		<b>9.8</b>	<b>8.5</b>	<b>11.9</b>	<b>15.5</b>	<b>19.5</b>	<b>22.8</b>
Chen <i>et al.</i> , [24]	-	Default	17.6	16.3	20.9	26.1	32.6	36.1
Chen <i>et al.</i> , [43]	-		13.3	11.7	16.3	20.7	25.6	29.3

magnitude features leads to clear improvements for MISO<sub>1</sub>. Using MISO based post-filtering that predicts target speakers one by one, MISO<sub>1</sub>-BF-MISO<sub>3</sub> yields large improvements over MISO<sub>1</sub>, especially for high overlap ratios (e.g. 8.6% vs. 13.8% WER on 40% overlap). MISO<sub>1</sub>-BF-MISO<sub>3</sub> also shows good enhancement performance. In the 0S and 0L conditions, it respectively obtains 5.5% and 5.9% WER, which are very close to the 4.9% and 5.1% WER of using the corresponding anechoic LibriSpeech signals for decoding (see the last row of Table II).

Table III reports the performance of monaural processing on the utterance-wise task of LibriCSS. Using magnitude features in SISO<sub>1</sub> leads to large improvement, for example from 15.5% to 9.5% WER in the 0S condition. The SISO<sub>1</sub>-SISO<sub>3</sub> system stacks two SISO networks, where SISO<sub>1</sub> resolves the permutation problem and SISO<sub>3</sub> predicts target speakers one by one by using  $\langle Y_q, \hat{S}_q^{(1)}(c) \rangle$  as inputs to estimate  $S_q(c)$ . Slight improvement is observed by using a second SISO network.

TABLE IV and TABLE V respectively present the continuous evaluation results on the seven- and one-channel tasks of LibriCSS. We observe that using magnitude features in MISO<sub>1</sub> and SISO<sub>1</sub> helps. MISO<sub>1</sub>+SC means the inclusion of a frame-level speaker counting branch in the MISO network, and we use the counting results for stream merging. Clear improvement is obtained by using speaker counting. Similar to utterance-wise evaluation, MISO<sub>1</sub>+SC-BF-MISO<sub>3</sub> produces much better performance over MISO<sub>1</sub>+SC.

Compared with monaural models, our seven-channel models yield large improvements in both utterance-wise and continuous evaluations. These results clearly demonstrate the effectiveness of DNN and MISO based time-varying non-linear beamforming and post-filtering, and most importantly, the



strong generalizability of our trained models to real arrays with the same geometry.

Based on the default ASR backend, our best seven-microphone frontend produces much better WER on LibriCSS over the current best results reported in [43], which uses magnitudes and IPDs to compute block-online masking based MVDR for separation. For example, on 40% overlap, MISO<sub>1</sub>+SC-BF-MISO<sub>3</sub> obtains 10.4% WER in continuous-input evaluation and MISO<sub>1</sub>-BF-MISO<sub>3</sub> gets 8.6% in utterance-wise evaluation, which are much better than 19.6% and 15.1% WER reported in [43]. We believe that MVDR alone cannot sufficiently suppress non-target speakers, although it maintains each target speaker distortionlessly. Our single-channel models, which combine a TCN with a dense U-Net for complex spectral mapping, also obtain better performance over the monaural ones in [24] and [43], which use BLSTM and conformer for real-valued T-F masking.

We further apply an end-to-end (E2E) ASR backend for utterance-wise evaluation. It uses a publicly available transformer-based model in ESPnet [46] trained on the LibriSpeech corpus. On the test-clean set of LibriSpeech, the model obtains 2.5% WER, which is slightly worse than the 2.08% WER obtained by the E2E ASR backend used in [43]. By applying our E2E backend to the utterance-wise separation results of [24], we achieve much better WER over the default backend, for example 9.9% vs. 21.6% in the condition of 40% overlap (see Table II). Combined with our frontend, the E2E backend gets overall better results than [43] (for example on 40% overlap, 4.6% vs. 6.2% WER in Table II and 15.5% vs. 17.1% in Table III), although the performance is slightly worse in the 0L condition.

## VI. CONCLUDING REMARKS

We have proposed a multi-microphone complex spectral mapping approach to address both speaker separation and dereverberation. The superior separation and ASR results on SMS-WSJ indicate that two-speaker separation in simulated reverberant conditions can now be addressed very well by exploiting the spectral and spatial information afforded by a fixed six-microphone array using frequency-domain methods, even though our study considers dereverberation in addition to separation and does not leverage extra information such as speaker embeddings and visual cues.

Time-domain approaches recently gain popularity in monaural speaker separation. On SMS-WSJ, our single-channel models show better PESQ, eSTOI and WER, and worse SI-SDR over monaural DP-RNN. Our multi-channel models obtain much better performance than FaSNet with TAC modules. Importantly, our models also produce strong recognition performance on the more realistic LibriCSS corpus.

Although trained on simulated RIRs, the proposed MISO and MISO-BF-MISO models generalize well to the real device used in LibriCSS. This is a significant finding, as it suggests that we can train models on simulated multi-channel conditions, which can be readily simulated, and expect them to generalize well to real devices with matched array geometry.

Our study shows that using the direct outputs from a strong DNN can produce much better ASR results over time-invariant

beamforming, at least in speaker separation in reverberant conditions with weak and relatively stationary noise. This finding contrasts that in single-speaker robust ASR [18], [47], where only one speaker is assumed active in noisy-reverberant environments. The reason could be that multi-talker speech is more harmful for recognition, and therefore frontend processing needs to dramatically suppress non-target speakers. In addition, competing speakers are easier to suppress as speech signal shows strong patterns unlike reverberation and noise. On the other hand, for single-speaker robust ASR, there is only one active speaker and speech distortion is more of a concern, as multi-condition training can deal with noise and reverberation to some extent. Future research shall consider multi-speaker ASR in reverberant conditions with challenging noises.

The major limitation of our current study for continuous speaker separation comes from the assumption that each short processing block contains at most two concurrent speakers. To deal with more than two speakers, we could just do say three- or four-speaker PIT, or use recursive separation [48] in each block. Another weakness is that the first MISO network needs to run  $P$  times, once for each microphone to compute the statistics for beamforming in order to get the best performance, resulting in high computational costs. One solution would be to replace it with a multi-microphone input and multi-microphone output network that can predict all the target speakers at all the microphones [26]. Another possible way is to run MISO only for the reference microphone and use mask-based beamforming [38], at a cost of some performance degradation.

## REFERENCES

- [1] J. R. Hershey, Z. Chen, J. Le Roux, and S. Watanabe, "Deep Clustering: Discriminative Embeddings for Segmentation and Separation," in *IEEE International Conference on Acoustics, Speech and Signal Processing*, 2016, pp. 31–35.
- [2] M. Kolbæk, D. Yu, Z.-H. Tan, and J. Jensen, "Multi-Talker Speech Separation with Utterance-Level Permutation Invariant Training of Deep Recurrent Neural Networks," *IEEE/ACM Trans. Audio, Speech, Lang. Process.*, vol. 25, no. 10, pp. 1901–1913, 2017.
- [3] Z.-Q. Wang, J. Le Roux, and J. R. Hershey, "Multi-Channel Deep Clustering: Discriminative Spectral and Spatial Embeddings for Speaker-Independent Speech Separation," in *IEEE International Conference on Acoustics, Speech and Signal Processing*, 2018, pp. 1–5.
- [4] Z.-Q. Wang and D. L. Wang, "Combining Spectral and Spatial Features for Deep Learning Based Blind Speaker Separation," *IEEE/ACM Trans. Audio, Speech, Lang. Process.*, vol. 27, no. 2, pp. 457–468, 2019.
- [5] T. Yoshioka, H. Erdogan, Z. Chen, and F. Alleva, "Multi-Microphone Neural Speech Separation for Far-Field Multi-Talker Speech Recognition," in *IEEE International Conference on Acoustics, Speech and Signal Processing*, 2018, pp. 5739–5743.
- [6] Y. Luo, Z. Chen, N. Mesgarani, and T. Yoshioka, "End-to-End Microphone Permutation and Number Invariant Multi-Channel Speech Separation," in *IEEE International Conference on Acoustics, Speech and Signal Processing*, 2020, pp. 6394–6398.
- [7] R. Gu et al., "Enhancing End-to-End Multi-Channel Speech Separation Via Spatial Feature Learning," in *IEEE International Conference on Acoustics, Speech and Signal Processing*, 2020, pp. 7319–7323.
- [8] Z.-Q. Wang, K. Tan, and D. L. Wang, "Deep Learning Based Phase Reconstruction for Speaker Separation: A Trigonometric Perspective," in *IEEE International Conference on Acoustics, Speech and Signal Processing*, 2019, pp. 71–75.
- [9] Y. Luo and N. Mesgarani, "Conv-TasNet: Surpassing Ideal Time-Frequency Magnitude Masking for Speech Separation," *IEEE/ACM Trans. Audio, Speech, Lang. Process.*, vol. 27, no. 8, pp. 1256–1266, 2019.
- [10] Y. Liu and D. L. Wang, "Divide and Conquer: A Deep CASA Approach to Talker-Independent Monaural Speaker Separation," *IEEE/ACM Trans.*

- Audio, Speech, Lang. Process.*, vol. 27, pp. 2092–2102, 2019.
- [11] Q. Wang *et al.*, “VoiceFilter: Targeted Voice Separation by Speaker-Conditioned Spectrogram Masking,” in *Proceedings of Interspeech*, 2019, vol. 2019-Sept, pp. 2728–2732.
  - [12] N. Zeghidour and D. Grangier, “Wavesplit: End-to-End Speech Separation by Speaker Clustering,” in *arXiv preprint arXiv:2002.08933*, 2020.
  - [13] A. Ephrat *et al.*, “Looking to Listen at the Cocktail Party: A Speaker-Independent Audio-Visual Model for Speech Separation,” *ACM Trans. Graph.*, vol. 37, no. 4, Apr. 2018.
  - [14] S. Gannot, E. Vincent, S. Markovich-Golan, and A. Ozerov, “A Consolidated Perspective on Multi-Microphone Speech Enhancement and Source Separation,” *IEEE/ACM Trans. Audio, Speech, Lang. Process.*, vol. 25, pp. 692–730, 2017.
  - [15] D. L. Wang and J. Chen, “Supervised Speech Separation Based on Deep Learning: An Overview,” *IEEE/ACM Trans. Audio, Speech, Lang. Process.*, vol. 26, pp. 1702–1726, 2018.
  - [16] J. Heymann, L. Drude, A. Chinaev, and R. Haeb-Umbach, “BLSTM Supported GEV Beamformer Front-End for The 3rd CHiME Challenge,” in *IEEE Workshop on Automatic Speech Recognition and Understanding*, 2015, pp. 444–451.
  - [17] T. Yoshioka *et al.*, “The NTT CHiME-3 System: Advances in Speech Enhancement and Recognition for Mobile Multi-Microphone Devices,” in *IEEE Workshop on Automatic Speech Recognition and Understanding*, 2015, pp. 436–443.
  - [18] J. Barker, R. Marxer, E. Vincent, and S. Watanabe, “The Third ‘CHiME’ Speech Separation and Recognition Challenge: Analysis and Outcomes,” *Comput. Speech Lang.*, vol. 46, pp. 605–626, 2017.
  - [19] P. Pertilä and E. Cakir, “Robust Direction Estimation with Convolutional Neural Networks Based Steered Response Power,” in *IEEE International Conference on Acoustics, Speech and Signal Processing*, 2017, pp. 6125–6129.
  - [20] Z.-Q. Wang, X. Zhang, and D. L. Wang, “Robust Speaker Localization Guided by Deep Learning Based Time-Frequency Masking,” *IEEE/ACM Trans. Audio, Speech, Lang. Process.*, vol. 27, no. 1, pp. 178–188, 2019.
  - [21] S. Chakrabarty and E. A. P. Habets, “Time-Frequency Masking Based Online Multi-Channel Speech Enhancement with Convolutional Recurrent Neural Networks,” *IEEE J. Sel. Top. Signal Process.*, 2019.
  - [22] S. Adavanne, A. Politis, J. Nikunen, and T. Virtanen, “Sound Event Localization and Detection of Overlapping Sources using Convolutional Recurrent Neural Networks,” *IEEE J. Sel. Top. Signal Process.*, vol. 13, no. 1, pp. 34–48, 2019.
  - [23] S. Chakrabarty and E. A. P. Habets, “Multi-Speaker DOA Estimation using Deep Convolutional Networks Trained with Noise Signals,” *IEEE J. Sel. Top. Signal Process.*, vol. 13, no. 1, pp. 8–21, 2019.
  - [24] Z. Chen *et al.*, “Continuous Speech Separation: Dataset and Analysis,” in *IEEE International Conference on Acoustics, Speech and Signal Processing*, 2020, pp. 7284–7288.
  - [25] L. Drude, J. Heitkaemper, C. Boeddeker, and R. Haeb-Umbach, “SMS-WSJ: Database, Performance Measures, and Baseline Recipe for Multi-Channel Source Separation and Recognition,” in *arXiv preprint arXiv:1910.13934*, 2019.
  - [26] Z.-Q. Wang and D. L. Wang, “Multi-Microphone Complex Spectral Mapping for Speech Dereverberation,” in *IEEE International Conference on Acoustics, Speech and Signal Processing*, 2020, pp. 486–490.
  - [27] D. S. Williamson, Y. Wang, and D. L. Wang, “Complex Ratio Masking for Monaural Speech Separation,” *IEEE/ACM Trans. Audio, Speech, Lang. Process.*, pp. 483–492, 2016.
  - [28] Z.-Q. Wang and D. L. Wang, “Deep Learning Based Target Cancellation for Speech Dereverberation,” *IEEE/ACM Trans. Audio, Speech, Lang. Process.*, vol. 28, pp. 941–950, 2020.
  - [29] Z.-Q. Wang, P. Wang, and D. Wang, “Complex Spectral Mapping for Single- and Multi-Channel Speech Enhancement and Robust ASR,” *IEEE/ACM Trans. Audio, Speech, Lang. Process.*, vol. 28, pp. 1778–1787, 2020.
  - [30] T. Nakatani, C. Boeddeker, K. Kinoshita, R. Ikeshita, M. Delcroix, and R. Haeb-Umbach, “Jointly Optimal Denoising, Dereverberation, and Source Separation,” *IEEE/ACM Trans. Audio Speech Lang. Process.*, vol. 28, pp. 2267–2282, 2020.
  - [31] X. Xiao *et al.*, “Deep Beamforming Networks for Multi-Channel Speech Recognition,” in *IEEE International Conference on Acoustics, Speech and Signal Processing*, 2016, pp. 5745–5749.
  - [32] Z. Zhang, Y. Xu, M. Yu, S.-X. Zhang, L. Chen, and D. Yu, “ADL-MVDR: All Deep Learning MVDR Beamformer for Target Speech Separation,” in *arXiv preprint arXiv:2008.06994*, 2020.
  - [33] D. Stoller, S. Ewert, and S. Dixon, “Wave-U-Net: A Multi-Scale Neural Network for End-to-End Audio Source Separation,” in *Proceedings of ISMIR*, 2018, pp. 334–340.
  - [34] N. Tawara, T. Kobayashi, and T. Ogawa, “Multi-Channel Speech Enhancement using Time-Domain Convolutional Denoising Autoencoder,” in *Proceedings of Interspeech*, 2019, pp. 86–90.
  - [35] C. Le Liu, S.-W. Fu, Y.-J. Li, J.-W. Huang, H.-M. Wang, and Y. Tsao, “Multichannel Speech Enhancement by Raw Waveform-Mapping using Fully Convolutional Networks,” *IEEE/ACM Trans. Audio Speech Lang. Process.*, vol. 28, pp. 1888–1900, 2020.
  - [36] Y. Luo, C. Han, N. Mesgarani, E. Ceolini, and S.-C. Liu, “FaSNet: Low-Latency Adaptive Beamforming for Multi-Microphone Audio Processing,” in *IEEE Workshop on Automatic Speech Recognition and Understanding*, 2019, pp. 260–267.
  - [37] J. Heitkaemper, D. Jakobeit, C. Boeddeker, L. Drude, and R. Haeb-Umbach, “Demystifying TasNet: A Dissecting Approach,” in *IEEE International Conference on Acoustics, Speech and Signal Processing*, 2020, pp. 6359–6363.
  - [38] Z.-Q. Wang, H. Erdogan, S. Wisdom, K. Wilson, and J. R. Hershey, “Sequential Multi-Frame Neural Beamforming for Speech Separation and Enhancement,” in *arXiv preprint arXiv:1911.07953*, 2020.
  - [39] D. Yu, M. Kolbæk, Z.-H. Tan, and J. Jensen, “Permutation Invariant Training of Deep Models for Speaker-Independent Multi-talker Speech Separation,” in *IEEE International Conference on Acoustics, Speech and Signal Processing*, 2017, pp. 241–245.
  - [40] S.-W. Fu, T.-Y. Hu, Y. Tsao, and X. Lu, “Complex Spectrogram Enhancement By Convolutional Neural Network with Multi-Metrics Learning,” in *IEEE International Workshop on Machine Learning for Signal Processing*, 2017, pp. 1–6.
  - [41] K. Tan and D. L. Wang, “Learning Complex Spectral Mapping With Gated Convolutional Recurrent Networks for Monaural Speech Enhancement,” *IEEE/ACM Trans. Audio, Speech, Lang. Process.*, vol. 28, pp. 380–390, 2020.
  - [42] U. Isik, R. Giri, N. Phansalkar, J.-M. Valin, K. Helwani, and A. Krishnaswamy, “PoCoNet: Better Speech Enhancement with Frequency-Positional Embeddings, Semi-Supervised Conversational Data, and Biased Loss,” in *Proceedings of Interspeech*, 2020.
  - [43] S. Chen *et al.*, “Continuous Speech Separation with Conformer,” in *arXiv preprint arXiv:2008.05773*, 2020.
  - [44] M. Pariente *et al.*, “Asteroid: The PyTorch-Based Audio Source Separation Toolkit for Researchers,” in *Proceedings of Interspeech*, 2020.
  - [45] Y. Luo, Z. Chen, and T. Yoshioka, “Dual-Path RNN: Efficient Long Sequence Modeling for Time-Domain Single-Channel Speech Separation,” in *IEEE International Conference on Acoustics, Speech and Signal Processing*, 2020, vol. 2020-May, pp. 46–50.
  - [46] S. Watanabe *et al.*, “ESPnet: End-to-End Speech Processing Toolkit,” in *Proceedings of Interspeech*, 2018, pp. 2207–2211.
  - [47] R. Haeb-Umbach, J. Heymann, L. Drude, S. Watanabe, M. Delcroix, and T. Nakatani, “Far-Field Automatic Speech Recognition,” *Proc. IEEE*, 2020.
  - [48] T. von Neumann *et al.*, “Multi-Talker ASR for An Unknown Number of Sources: Joint Training of Source Counting, Separation and ASR,” in *Proceedings of Interspeech*, 2020.
  - [49] C. Wang *et al.*, “Semantic Mask for Transformer Based End-to-End Speech Recognition,” in *arXiv preprint arXiv:1912.03010*, 2019.